journal

J. Am. Ceram. Soc., 94 [8] 2613–2618 (2011)
DOI: 10.1111/j.1551-2916.2011.04471.x

Quantitative Analysis of Crack Closure Driven by Laplace Pressure in Silica Glass

Gaël Pallares,[‡,§] Antoine Grimaldi,[‡] Matthieu George,[†,‡] Laurent Ponson,[¶,‖] and Matteo Ciccotti[‡,‡‡]

[‡]Laboratoire des Colloïdes, Verres et Nanomatériaux, CNRS, Université Montpellier 2, France

[§]CEA, IRAMIS, SPCSI, Grp. Complex Systems & Fracture, F-91191 Gif Sur Yvette, France

[¶]Division of Engineering and Applied Science, California Institute of Technology, Pasadena, California 91125

[‖]CNRS and UPMC Univ Paris 06, UMR 7190, Institut Jean le Rond d'Alembert, F-75005 Paris, France

[‡‡]Laboratoire PPMD-SIMM, UMR 7615, ESPCI, CNRS, Université Paris 6, France

Crack tips in silica glass in moist atmosphere are filled with an equilibrium liquid condensation of a few hundred nanometers length. Not only does this local environment affect the chemistry of slow crack propagation by stress corrosion, but it also has an important mechanical effect due to its highly negative Laplace pressure. The present article presents an original technique for measuring the physical properties of the liquid condensation in terms of the Laplace pressure and critical condensation distance. This is achieved by combining *in situ* atomic force microscopy measurements of the condensate length and optical determination of the crack closure threshold in a double cleavage drilled compression specimen.

I. Introduction

Crack tips in silicate glasses in moist atmosphere are invariably filled with a stable liquid phase, mainly composed of water, because of the phenomenon of capillary condensation. This is due to the extremely hydrophilic nature of glass surfaces, which are perfectly wet by water and to the elevated stiffness of glass that makes cracks very sharp, the crack opening remaining limited to less than a few nanometers up to a distance of hundreds of nanometers to few micrometers. Macroscopic failure properties of materials being essentially governed by mechanisms taking place in the vicinity of the crack tip, such a liquid condensate has a potential for playing an important role on the propagation of the crack, in spite of its submicronic extension. First, it affects the chemistry allowing crack propagation at low velocity by determining the local environmental condition for the stress-corrosion reactions at the crack tip. But it can also have a mechanical effect due to the highly negative Laplace pressure in the condensate that acts on the crack walls and is responsible for the closure of the crack when the stress becomes lower than some threshold.

Although the presence of capillary menisci in glass fractures have been previously argued[1,2] for elevated relative humidity, proper characterization by *in situ* atomic force microscopy (AFM) measurements has only been recently achieved.[3,4] An original application of AFM phase imaging techniques has made it possible to measure the length L of the condensate as a function of the stress intensity factor (SIF) K, that controls the crack opening profile.[††] For silica glass the condensation was shown to be at equilibrium with an atmosphere of moist nitrogen and the critical condensation distance H_c was measured for several values of the relative humidity.[5] Silica glass is particularly suited to investigate the physico-chemical properties of the capillary condensate because the stress-corrosion reaction does not involve corrosion products or ion exchange phenomena.

When measuring the $K-L$ curves by AFM phase imaging as in Grimaldi *et al.*,[5] the range of measurable values are insufficient for estimating the Laplace pressure. It was shown that neglecting the mechanical effect of the Laplace pressure on the crack opening profile induces a bias in the estimate of the critical distance H_c which was limited to within 15%.[6] The present work presents an important extension of the previous technique, which allows the concomitant determination of both the critical condensation distance H_c and the Laplace pressure $-\Delta P$ in the condensate,[‡‡] and thus leads to a complete unbiased characterization of the physical properties of the wetting liquid.

II. Mechanical Effect of Capillary Forces

When a hydrophilic solid is in equilibrium with a moist atmosphere, capillary condensation is expected to fill all gaps which are smaller than the critical distance H_c, that can be related to the Kelvin radius and to the wetting properties.[7] For a sharp crack with an opening profile $f(X)$, this implies a condensation length L given by the condition (cf. Fig. 1)

$$f(X = L) = H_c \tag{1}$$

When neglecting the effect of capillary forces, the crack opening profile can be modeled according to the Irwin solution[§§]:

$$\delta = 2u_y(X, 0) = f(X) = \frac{2K}{E'}\sqrt{\frac{8X}{\pi}} \tag{2}$$

where E' is an effective elastic modulus,[¶¶] X the distance from the crack tip and $u_y(X,0)$ the elastic displacement of the crack lips. Using Eq. (1), we obtain the following relation for equilibrium

T. Rouxel—contributing editor

Manuscript No. 28640. Received September 21, 2010; approved February 2, 2011.
This work was supported by the ANR Grant "Corcosil" No. ANR-07-BLAN-0261-02. L. Ponson is supported by the European Union through the "Phycracks" Marie Curie fellowship.
[†]Author to whom correspondence should be addressed. e-mail: mgeorge@univ-montp2.fr

[††]The symbol K will stand for the macroscopic mode I stress intensity factor. When making the difference between external end internal forces, this will be called K_{Ext}.

[‡‡]The Laplace pressure $-\Delta P$ ($\Delta P>0$) is the difference between the pressure of the condensed liquid phase and the moist atmosphere at equilibrium. The pressure in the condensate is assumed to be constant and independent of the crack profile geometry because its value is governed by the radius of curvature of the meniscus that is a function of relative humidity. In addition, the fluid is at rest in the condensate, insuring a homogeneous pressure.

[§§]The Irwin solution is only valid in a close neighborhood of the crack tip, which is estimated to $X<15$ μm in the Appendix for our sample geometry. This is comfortably satisfied since the observed condensate lengths are always smaller than 4 μm.

[¶¶]$E' = E/(1-\upsilon^2)$ refers here to the plane strain Young's modulus. Indeed, we make such an assumption in our 2D model since most of the measurements such as the crack closure conditions will be measured in the mid plane of the sample, where such plane strain conditions prevail. The characterization of the condensate properties at the free surface of the sample will be justified in the discussion part.

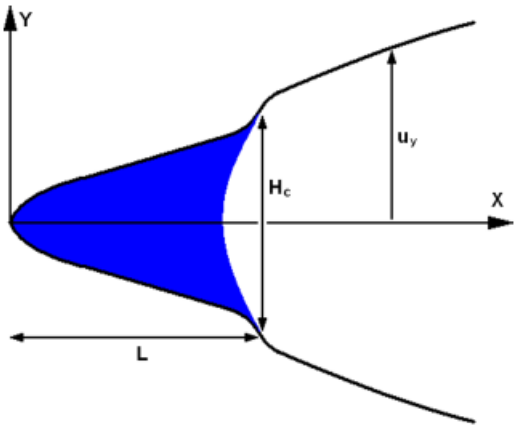

Fig. 1. Schematic representation of an open crack showing how a capillary condensate modifies the crack opening profile near the crack tip.

K–L curves:

$$L(K, H_c) = \frac{\pi}{8}\left(\frac{E' H_c}{2K}\right)^2 \tag{3}$$

that was used by Grimaldi *et al.*[5] to estimate H_c without knowing the Laplace pressure. This relation has the form of an inverse square dependence of L on the SIF K and does not account for a closure threshold.

Capillary forces can be modeled as the action of a constant internal negative Laplace pressure $-\Delta P$ between the crack lips when the crack opening is less than a distance H_c:

$$\sigma_{yy} = \begin{cases} -\Delta P & \delta \le H_c \\ 0 & \delta > H_c \end{cases} \tag{4}$$

i.e. when the distance X from the crack tip is less than L. This internal force distribution is completely equivalent to the Dugdale formalism for the cohesive zone in ductile fracture,[8] and thus presents the same solutions. The solutions for the crack opening profile can be written as the superposition of two terms, respectively, related to the external and internal forces[‖‖]:

$$K_{Tot} = K_{Ext} + K_{Int} \qquad u_y^{Tot} = u_y^{Ext} + u_y^{Int} \tag{5}$$

For small condensate length,[***] the contribution of the internal forces can be written as[8]:

$$K_{Int} = -\sqrt{\frac{2}{\pi}}\Delta P \int_0^L \frac{dX}{\sqrt{X}} = -\Delta P\sqrt{\frac{8L}{\pi}} \tag{6}$$

$$u_y^{Int}(X,0) = \frac{K_{Int}}{E'}\sqrt{\frac{8X}{\pi}} - \frac{1}{2}\frac{K_{Int}}{E'}\sqrt{\frac{8L}{\pi}} \times \left[\sqrt{\frac{X}{L}} - \frac{1}{2}\left(1 - \frac{X}{L}\right)\ln\left|\frac{\sqrt{\frac{X}{L}}+1}{\sqrt{\frac{X}{L}}-1}\right|\right] \tag{7}$$

The new condensation length can be obtained by applying the condition (1) to these new solutions.[†††] The equilibrium K_{Ext}–L curve becomes:

$$2u_y(L) = \frac{2K_{Ext} + K_{Int}}{E'}\sqrt{\frac{8L}{\pi}} = H_c \tag{8}$$

This modeling predicts a crack closure threshold K_0 when the condition $K_{Tot} = K_{Ext} + K_{Int} = 0$ is satisfied, i.e. $K_{Int} = -K_{Ext} = -K_0$. By combining Eqs. (6) and (8), the threshold can be expressed as:

$$K_0 = \sqrt{E' H_c \Delta P} \tag{9}$$

This can be easily related to the adhesion energy[9]:

$$G_0 = w = \int_0^\infty \sigma_{yy} du_y = \int_0^{H_c} \Delta P du_y = \Delta P H_c \tag{10}$$

by using the equivalence $G_0 = K_0^2/E'$. At crack closure, the condensate length assumes a maximum value L_{max} given by

$$L_{max} = \frac{\pi}{8}\frac{E' H_c}{\Delta P} = \frac{\pi}{8}\frac{K_0^2}{\Delta P^2} \tag{11}$$

Let us note that the leading term proportional to $\sqrt{X}$ in the development of the crack profile vanishes at the onset of crack closure, so that the crack opening evolves as $u_y(X) \approx \frac{K_{Ext}}{E'}\frac{2}{\pi}\frac{X^{3/2}}{L}$ in the vicinity of the tip for $K_{Ext} = K_0$. We remark that K_0 and L_{Max} naturally constitute two characteristic values for K and L, emerging from the values of E', H_c, and ΔP. The K_{Ext}–L curves (8) can thus be expressed in an elegant dimensionless form[‡‡‡]:

$$\frac{L}{L_{max}} = \left(\frac{K_{Ext}}{K_0} - \sqrt{\left(\frac{K_{Ext}}{K_0}\right)^2 - 1}\right)^2 \tag{12}$$

In the limit of large loadings ($K_{Ext} \gg K_0$), we recover from this formula the variations of $L \propto 1/K_{Ext}^2$ found when the mechanical effect of the condensate is neglected (Eq. [3]). As discussed previously, it is difficult to adjust both parameters by only using the K_{Ext}–L curves determined by AFM phase imaging. However, if the closure threshold K_0 is measured independently, it is then easy to adjust the parameter L_{max} on the K_{Ext}–L curves. This allows an unbiased and robust measurement of both the critical condensation distance H_c and the Laplace pressure according to the inverse relations:

$$\Delta P = K_0\sqrt{\frac{\pi}{8L_{max}}} \qquad H_c = \frac{K_0}{E'}\sqrt{\frac{8L_{max}}{\pi}} \tag{13}$$

III. Experimental Procedure and Results

(1) In Situ Monitoring of Slow Crack Propagation

Fractures are initiated and propagated on a double cleavage drilled compression (DCDC) setup[10] at a constant temperature of (25.5±0.5)°C in a leak-proof chamber under an atmosphere composed of air and water vapor at a given relative humidity level $RH = (39 \pm 2)\%$. The parallelepipedic DCDC samples (4 mm × 4 mm × 40 mm, with 10 μm tolerance) of pure silica glass (Suprasil 311, Heraeus, Hanau, Germany) were polished to

[‖‖]The procedure used here closely follows the approach described in Lawn (1993) p. 59.[2] The problem is solved as the superposition of two solutions. The superscript "Ext" refers to the solution where only the external forces are applied, i.e. the macroscopic forces applied to the sample grips, as in Eq. (2). The superscript "Int" refers to the solution where only the internal forces are applied, i.e. the microscopic capillary forces acting between the crack lips. The superscript "Tot" refers to the sum of these two solutions, which corresponds to the real problem. We should stress that the term K_{tot} corresponds to the loading felt by the silica at the crack tip.

[***]This corresponds to the small size yield approximation of the Dugdale model. The domain of validity of this approximation is $L < 5$ μm (cf. Appendix), which is also satisfied.

[†††]The term in brackets in Eq. (7) can be easily verified to equal unity for $X = L$.

[‡‡‡]Multiplying Eq. (8) by ΔP, we obtain:

$$E' H_c \Delta P = (2K_{Ext} + K_{Int})\Delta P\sqrt{\frac{8L}{\pi}}$$
$$K_0^2 = (2K_{Ext} + K_{Int})(-K_{Int})$$
$$K_{Int}^2 + 2K_{Int}K_{Ext} + K_0^2 = 0$$
$$K_{Int} = -K_{Ext} + \sqrt{K_{Ext}^2 - K_0^2} = -\Delta P\sqrt{\frac{8L}{\pi}}$$

and using Eq. (11), we easily obtain the dimensionless form (12).

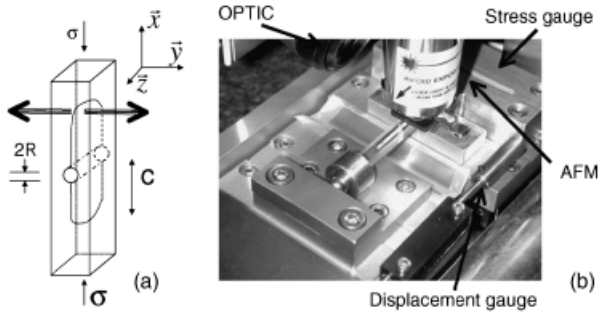

Fig. 2. Experimental setup: (a) Sketch of the double cleavage drilled compression geometry; (b) picture of the experiment.

a RMS roughness of 0.25 nm (for an area of 10 μm × 10 μm) and a hole of radius $R = 0.5$ mm was drilled at their center to trigger the initiation of two symmetric fractures of length c shown in Fig. 2. The hole's radius is evaluated precisely for each sample by optical microscopy.

For an applied external compressive stress σ, the SIF K_{Ext} is determined as a function of the crack length according to the Eq. (A-1) in the Appendix A. By coupling optical and AFM (Nanoscope 3a, VeecoMetrology Inc., Santa Barbara, CA), the crack propagation velocity can be measured from 10^{-12} to 10^{-5} m/s. The details of the technique can be found in Celarié.[11]

(2) Measurement of Condensate Length by AFM Phase Imaging

AFM observations are performed in tapping mode with AFM tips having a nominal radius of $R_{tip} \sim 10$ nm (DNP, MPP-11100-10, Veeco Metrology Inc., Camarillo, CA). The tip is oscillated at constant frequency ω (close to the resonance frequency ω_0). The oscillation amplitude A is kept constant to a set value thanks to a feedback loop controlling the vertical position of the scanner. The phase delay ($\vartheta \in [-\pi : 0]$) between the stimulation and the oscillation of the tip can be related to the energy E_D dissipated per cycle by the tip-surface interactions[12]:

$$E_D = \frac{\pi k A^2}{Q}\left(-\frac{A}{A_0}\sin\vartheta - \frac{\omega}{\omega_0}\right) \tag{14}$$

where k, Q, A_0 are respectively the stiffness of the AFM cantilever, the quality factor, and the free resonance amplitude.

Figure 3 shows typical height and phase images of the crack tip. The crack plane intersects perpendicularly the observed external surface of the sample. The region along the crack, characterized by a strong phase contrast, corresponds to the portion of the crack, which is filled by a condensed liquid phase. According to Eq. (14), the phase contrast on the condensate region corresponds to an increase in the energy dissipated by the tip-sample interaction.[4] Under humidity, the presence of thin water

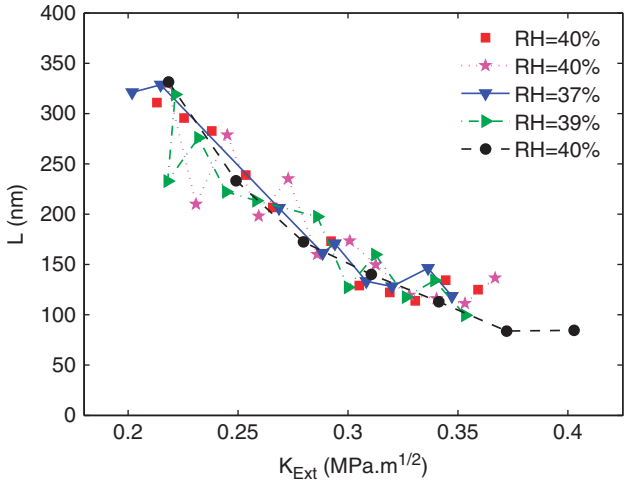

Fig. 4. Condensate length L as a function of the stress intensity factor K_{Ext} obtained by atomic force microscopy.

films on both the external sample surface and the AFM tip entails energy dissipation due to the combination of two phenomena: (1) the formation and rupture of a capillary bridge at each oscillation of the AFM tip[13] and (2) the visco-elastic displacement in the thin films.[14] The dissipated energy is very weak when scanning the glass surface, but it is greatly enhanced when the AFM tip crosses a portion of the crack tip filled with liquid water.[4] The resolution of the AFM technique does not allow to measure the opening of the crack accurately (a few nanometers here), but it allows to measure the length L of the condensed region, ranging between 100 and 400 nm in our experiments, with an incertitude lower than 10 nm. Each estimate of the condensate length L is the average of three measurements on images with an optimized scan size. The measurement was shown not to be dependent on the AFM working conditions, or on the details of the AFM tip shape and its chemical nature within the given incertitude. The weak crack propagation velocity during the test was shown previously not to affect the equilibrium length of the condensate.[5] In order to avoid aging phenomena and to provide an optimum mode I loading condition, it is preferable to make each determination of the $K_{Ext}-L$ curve on a new specimen just after the crack initiation. The results are reported in Fig. 4 for five different samples and we remark an excellent reproducibility.

(3) Measurement of Crack Closure Threshold by Optical Microscopy

It is well known that when the external stress is reduced below some threshold, cracks in glass are observed to close progressively.[15,16] In order to perform the measurement of the crack closure by using the same loading setup and the

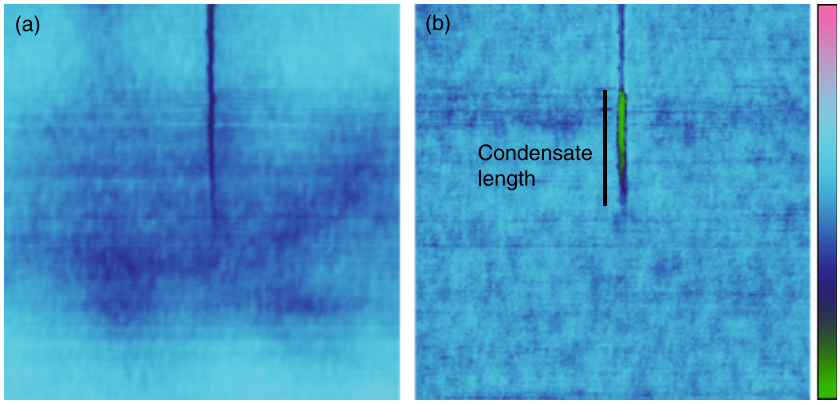

Fig. 3. Typical atomic force microscopy (AFM) height (a) and phase (b) images of the crack tip for a crack propagating from top to bottom of the image (400 nm × 400 nm). The scale range is respectively 5 nm and 5°.

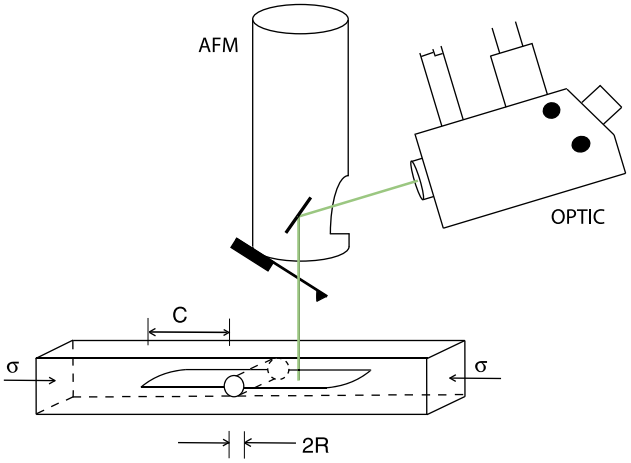

Fig. 5. Sketch of the double cleavage drilled compression sample arranged to observe the crack closure by optical microscopy (horizontal crack plane).

same environmental conditions as for the $K_{Ext}-L$ curves, we can use the optical microscope associated to the AFM system. When measuring $K_{Ext}-L$ curves, the crack front is vertical in order to image the crack tip by AFM at the free surface of the sample (cf. Fig. 2). In order to observe the crack closure, the DCDC sample is rotated by 90°, the fracture front laying horizontally according to Fig. 5. The white light source illuminates the sample vertically, after passing through the optical axis of the CCD camera and after being reflected by an inclined mirror in the AFM head. The field of view of the camera is 920 μm and the resolution is limited by the pixel size to 10 μm.

For the same reasons discussed for $K_{Ext}-L$ curves, it is again preferable to make each determination of the closure threshold on a new specimen just after the crack initiation. The new crack is propagated for a convenient crack length ($c > w = 2$ mm) until the propagation velocity becomes less than 10^{-9} m/s in order to avoid any further optically observable propagation during the measurement. Then, we continuously decrease the stress to a rate of 0.12 MPa/s and monitor the evolution of the crack front position, and thus the crack length, with an acquisition frequency of one image/second as reported in Fig. 6.

According to the modeling proposed in Section II, the crack opening profile undergoes two regimes: in the first stage of unloading the crack length will remain constant, while the crack

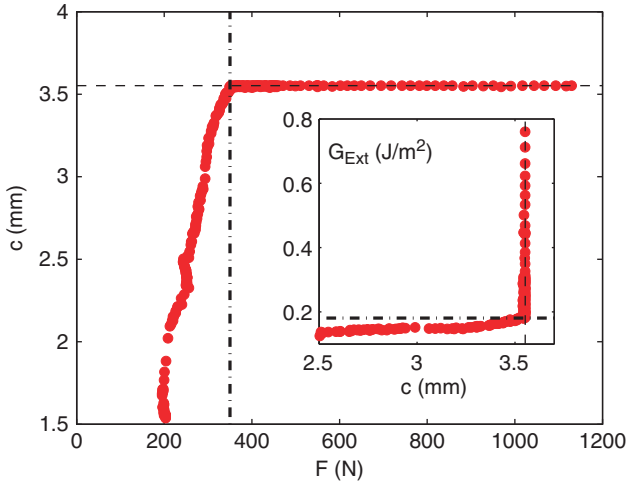

Fig. 6. Evolution of the apparent crack length c as a function of the external decreasing load F. In the inset, the same data are plotted in terms of the strain energy release rate $G_{Ext} = K_{Ext}^2/E'$ as a function of the apparent crack length c (NB: the axes are switched because c should now be considered as the independent variable). The crack closure threshold G_0 corresponds to the intersection between the two regimes.

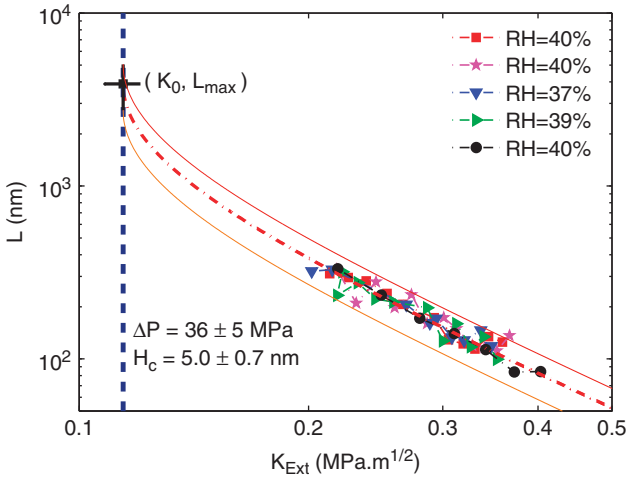

Fig. 7. Fit of the $K_{Ext}-L$ curve according to Eq. (12). The atomic force microscopy (AFM) measurements of Fig. 4 are combined with the optical measurements of the threshold K_0 (vertical dashed line). The black square symbol corresponds to the estimated value of L_{max}.

opening profile is progressively reduced and the condensate length increased. When the external SIF reaches the threshold value K_0, the contribution of internal and external forces is perfectly balanced, the crack tip singularity vanishes and the condensate length assumes the maximum value L_{max}. By further decreasing the external load the system enters another regime where the crack closes progressively. The threshold value K_0 is then accurately determined by measuring the load and the crack length[§§§] at the transition point (Fig. 6). The average over three tests in moist atmosphere with $RH = (40 \pm 3)\%$ is:

$$K_0 = (0.114 \pm 0.006)\ \text{MPa} \cdot \text{m}^{1/2} \quad G_0 = (180 \pm 20)\ \text{mJ/m}^2$$

where we used the elastic moduli of silica glass[¶¶¶] $E = (72 \pm 2)$ GPa and $\upsilon = (0.170 \pm 0.005)$.

(4) Estimate of the Laplace Pressure

Although none of the previous techniques allows the complete solution of the problem, their combination does. Indeed, we can insert the measured value of $K_0 = (0.114 \pm 0.006)\ \text{MPa} \cdot \text{m}^{1/2}$ into Eq. (12) and adjust the single missing parameter L_{max} on the $K_{Ext}-L$ curves. The fit is well conditioned and the result is shown in Fig. 7. We find:

$$L_{max} = (4 \pm 1)\ \mu\text{m}$$

By using Eq. (13) we determine the values of the critical distance H_c and of the Laplace pressure ΔP:

$$H_c = (5.0 \pm 0.7)\ \text{nm} \quad \Delta P = (36 \pm 5)\ \text{MPa}$$

IV. Discussion and Conclusion

Although several measurements exist in the literature for the closure threshold in glass,[15,16,18,19] it is the first time that they are combined with an *in situ* observation of the length of a liquid condensate. This allows us both a sound physical interpretation of the crack closure phenomenon and a complete characterization

[§§§] The exact position of the crack tip can not be perceived optically since the reflectivity of the glass-water interface is very weak, but L_{max} will be shown to be of the order of 4 μm, which is smaller than the optical resolution.

[¶¶¶] Silica glass is known to exhibit nonlinear elastic deformations according to[17]:

$$\frac{\Delta E}{E} = (1 + 5.75\varepsilon)$$

However, in the present analysis, the crack tip stresses are limited by the Laplace pressure $\Delta P \sim 40$ MPa ($\varepsilon \sim 0.05\%$). The maximum effect on the elastic modulus is thus of the order of 0.3%, which is negligible for our purposes.

of the physical parameters of the wetting liquid in terms of its Laplace pressure and critical condensation distance.

The value of the adhesion energy $G_0 = (180 \pm 20)$ mJ/m^2 is in good agreement with other determinations in the literature ranging between 100 and 200 mJ/m^2 (ibid.), which are generally roughly compared with the energy required to create two water surfaces ($2\gamma_w \sim 144$ mJ/m^2). According to more sophisticated modeling,[7] the adhesion energy in perfect wetting conditions is expected to exceed the surface tension term.

Our simple modeling accounts for the crack closure by the action of capillary forces and it neglects other kinds of interactions between the solid surfaces. This is also in agreement with the observed independence of the closure threshold on the glass nature,[16] and with similar conjectures formulated by Rayleigh[20] and Lawn *et al.*[19] Several other interpretations of the crack closure have been proposed ranging from hydrogen bond interaction between adsorbed water molecules to alkali ion bridging or partial reformation of SiOSi bonds between opposite crack surfaces.[15] However, they result from observations of the crack closure behavior on alkali containing glasses after several aging or thermal treatments. The present study avoids all ambiguity because it is performed on freshly fractured silica glass samples in very clean conditions. Although the cracks were produced by stress-corrosion, no corrosion products are expected at ambient conditions in silica because the silanol groups remain bonded to the crack walls and our $K_{Ext}-L$ measurements were stable on several days periods. In a previous paper,[5] we reported larger values for the condensate length and critical distance, but these were taken on a sample that had been aged for 1 year in primary vacuum. A detailed study of the aging behavior is out of the scope of the present work and will be published later.

It is the first time that the Laplace pressure is measured for a capillary condensation inside a crack tip. We remark that the reported value $\Delta P = (36 \pm 5)$ MPa corresponds to a very negative pressure inside the liquid phase and the remarks given above suggest that this condensed phase is very close to pure water. The stability of this phase is provided by the high degree of confinement which prevents nucleation of vapor bubbles.[21] Although the largest reported measured negative pressures are around -140 MPa,[22] the most reliable ones are around -20 MPa.[23] By combining this technique with a low humidity environmental chamber, it will be possible to obtain important data on the behavior of water at very negative pressure.[24,25]

An important remark concerns the opportunity of comparing $K_{Ext}-L$ curves that are measured at the sample surface with threshold measurements performed by observing the crack front in the bulk of the sample. Our modeling of the mechanical behavior of the DCDC sample, and in particular, the determination of the value of SIF, has been performed by a two dimensional plane strain analysis, which in the bulk describes accurately the behavior of the specimen. However, the recent application of digital image correlation techniques to the measurement of the surface displacement fields near the crack tip in our DCDC specimens have shown en excellent agreement between the values of the SIF determined at the surface and the values determined by a macroscopic determination according to two dimensional models of the DCDC sample.[26]

Incidentally, we remarked a significant hysteresis between the closure and reopening behavior of the crack as observed previously in Michalske and colleagues.[15,16,20] Moreover, while our equilibrium modeling would predict a constant SIF during the progression of the crack closure, a decrease of the threshold is observed during the closure at constant load rate (cf. Fig. 6), followed by a progressive increase when the loading process is arrested. These observations suggest the presence of irreversible processes that are not simply related to a velocity dependence as suggested in Stavrinidis and Holloway.[16] For that reason, we limited our determination of the threshold to the onset of the first closure, while leaving these interesting observations to future investigations.

The present results cast a clearer light on the physical mechanisms of crack closure in glasses, which are intimately related to the capillary forces. The elevated stiffness of these materials along with the high degree of chemical inertness of silica glass have allowed original and reproductible measurements of the condensate length. This precious ingredient, combined with the measurement of the adhesion energy through the crack closure threshold, allows obtaining an estimate of the Laplace pressure, and thus a complete characterization of the physical properties of the condensed phase.

Acknowledgments

We thank E. Charlaix, M. Flemming and T. Fett for fruitful discussions.

Appendix A

(A.1) 2D Modeling of the DCDC Specimen and Small Condensate Approximation

For a DCDC specimen of dimensions $2w \times 2t \times 2\ell$, containing a hole of radius R and two symmetric cracks of length c (cf. Fig. 2), the SIF K_{Ext} caused by the external loading $\sigma = F/4wt$ can be accurately approximated by the following dimensionless expansion in terms of the ratios c/R and w/R[27]:

$$\frac{\sigma\sqrt{\pi R}}{K_{Ext}} = \left[C_0 + C_1\frac{w}{R} + C_2\left(\frac{w}{R}\right)^2\right] + \left[C_3 + C_4\frac{w}{R} + C_5\left(\frac{w}{R}\right)^2\right]\frac{c}{R} \tag{A-1}$$

with the set of parameters: $C_0 = 0.3156$, $C_1 = 0.7350$, $C_2 = 0.0346$, $C_3 = -0.4093$, $C_4 = 0.3794$, and $C_5 = -0.0257$ for $2.5 \le w/R \le 5$ and $w < c < \ell - 2w$. For our geometry, this reduces to:

$$\frac{\sigma\sqrt{\pi R}}{K_{Ext}} = 3.547 + 0.650\frac{c}{R} \tag{A-2}$$

In the absence of internal forces, the crack opening profile was shown[27] to be described by a fifth order Williams expansion[28] with 1% accuracy when $X < 0.85\ w = 1.7$ mm:

$$u_y(X) = \frac{K_I}{E'}\sqrt{\frac{8}{\pi}}\sqrt{X} \times \left(1 + 1.319\left(\frac{X}{w}\right) + 0.515\left(\frac{X}{w}\right)^2\right) \tag{A-3}$$

This expression remains valid as far as the effects of the finite size of the specimen are not relevant, i.e. for $2.5w - R < c < L - 2.3w - R$. The range of 1% validity of the first order term, corresponding to the Irwin Eq. (2) used in the present work, is thus $X < 0.0076w = 15$ μm.[27]

The SIF caused by a generic distribution of internal forces along the crack faces can be calculated according to the weight function procedure developed by Bueckner[29]:

$$K_{Int} = \int_0^c h(c, X)\sigma_{yy}(X)dX \tag{A-4}$$

where the weight function $h(c, X)$ does not depend on the stress distribution, but only on the geometry of the specimen. The mode I weight function for the DCDC geometry were approximated by Fett *et al.*[30] by finite element simulation, and can be rewritten according to our formalism:

$$h_1(c, X) = \sqrt{\frac{2}{\pi X}}\left(1 + D_1^{(I)}\frac{X}{c} + D_2^{(I)}\left(\frac{X}{c}\right)^2\right) \tag{A-5}$$

where $D_1^{(I)}$ and $D_2^{(I)}$ were fitted by the following developments in the range $0 \leq c/R \leq 8$:

$$D_1^{(I)} = -3.97 + 1.466\frac{c}{R} + 4.533\exp\left(-0.291\frac{c}{R}\right)$$
$$D_2^{(I)} = -0.246 + 0.222\frac{c}{R} + 0.529\exp\left(-2.08\frac{c}{R}\right) \quad \text{(A-6)}$$

In our measurements, the crack length ranges between 3 and 5 mm, corresponding to c/R ranging between 5.66 and 9.43. Although the upper end is slightly higher than the domain where the former development where adjusted, the behavior of the Eq. (A-6) is quite linear near $c/R = 8$. It is thus raisonnable to extrapolate for estimate purpose the values $D_1^{(I)} = 10.152$ and $D_2^{(I)} = 1.848$ that correspond to the largest corrections. The range of 1% validity of the small condensate approximation, corresponding to the first term of Eq. (A-5) is thus $X < 5$ μm for our DCDC geometry. Because this domain of validity is always larger than the condensate length, this justifies the use of a global first-order approximation in all our modeling.

References

[1]S. N. Crichton, M. Tomozawa, J. S. Hayden, T. I. Suratwala, and J. H. Campbell, "Subcritical Crack Growth in a Phosphate Laser Glass," *J. Am. Ceram. Soc*., **82** [11] 3097–104 (1999).

[2]B. R. Lawn, *Fracture of brittle solids*, 2nd edition, Cambridge University Press, Cambridge, 1993.

[3]L. Wondraczek, A. Dittmar, C. Oelgardt, F. Célarié, M. Ciccotti, and C. Marlière, "Real-Time Observation of Non-Equilibrium Liquid Condensate Confined at Tensile Crack Tips in Oxide Glasses," *J. Am. Ceram. Soc*., **89** [2] 746–9 (2006).

[4]M. Ciccotti, M. George, V. Ranieri, L. Wondraczek, and C. Marlière, "Dynamic Condensation of Water at Crack Tips in Fused Silica Glass," *J. Non Cryst. Solids*, **354** [2–9] 564–8 (2008).

[5]A. Grimaldi, M. George, G. Pallares, C. Malière, and M. Ciccotti, "The Crack Tip: A Nanolab for Studying Confined Liquids," *Phys. Rev. Lett*., **100** [16] 165505 (2008).

[6]M. Ciccotti, G. Pallares, L. Ponson, A. Grimaldi, and M. George, "Mechanical Effect of Capillary Forces in the Crack Tip of a DCDC Specimen"; in *Proceedings of the 12th International Conference on Fracture*, Ottawa, Canada, 2009.

[7]E. Charlaix and M. Ciccotti, "Capillary Condensation in Confined Media"; pp. 12–1 in *Handbook of Nanophysics: Principles and Methods*, Edited by K. Sattler. CRC Press, Boca Raton, FL, 2010.

[8]D. S. Dugdale, "Yielding of Steel Sheets Containing Slits," *J. Mech. Phys. Solids*, **8** [2] 100–4 (1960).

[9]S. J. Burns and B. R. Lawn, "A Simulated Crack Experiment Illustrating Energy Balance Criterion," *Int. J. Frac. Mech*., **4** [3] 339–45 (1968).

[10]M. Y. He, M. R. Turner, and A. G. Evans, "Analysis of the Double Cleavage Drilled Compression Specimen for Interface Fracture Energy Measurements Over a Wide Range of Mode Mixities," *Acta Metall. Mater*., **43** [9] 3453–8 (1995).

[11]F. Celarié, "Dynamique de fissuration à basse vitesse des matériaux vitreux"; Ph.D. Thesis, Université Montpellier 2, France, 2004.

[12]J. P. Cleveland, B. Anczykowski, A. E. Schmid, and V. B. Elings, "Energy Dissipation in Tapping-Mode Atomic Force Microscopy," *Appl. Phys. Lett*., **72** [20] 2613–5 (1998).

[13]L. Zitzler, S. Herminghaus, and F. Mugele, "Capillary Forces in Tapping Mode Atomic Force Microscopy," *Phys. Rev. B*, **66** [15] 155436 (2002).

[14]L. Nony, T. Cohen-Bouhacina, and J. P. Aimé, "Dissipation Induced by Attractive Interaction in Dynamic Force Microscopy: Contribution of Adsorbed Water Layers," *Surf. Sci*., **499** [2–3] 152–60 (2002).

[15]T. A. Michalske and E. R. Fuller, "Closure and Repropagation of Healed Cracks in Silicate Glass," *J. Am. Ceram. Soc*., **68** [11] 586–90 (1985).

[16]B. Stavrinidis and D. G. Holloway, "Crack Healing in Glass," *Phys. Chem. Glasses*, **24** [1] 19–25 (1983).

[17]R. Brückner, "Properties and Structure of Vitreous Silica," *J Non-Cryst. Solids*, **5** [3] 123–75 (1971).

[18]S. M. Wiederhorn and P. R. Townsend, "Crack Healing in Glass," *J. Am. Ceram. Soc*., **53** [9] 486–9 (1970).

[19]K. T. Wan, D. T. Smith, and B. R. Lawn, "Fracture and Contact Adhesion Energies of Mica–Mica, Silica–Silica and Mica–Silica Interfaces in Dry and Moist Atmospheres," *J. Am. Ceram. Soc*., **75** [3] 667–76 (1992).

[20]L. Rayleigh, "Optical Contact," *Nature*, **139**, 781–3 (1937).

[21]J. N. Israelachvili, *Intermolecular and Surface Forces*, 2nd edition, Academic Press, New York, 1992.

[22]Q. Zheng, D. J. Durben, G. H. Wolf, and C. A. Angell, "Liquids at Large Negative Pressures—Water at the Homogeneous Nucleation Limit," *Science*, **254**, 829–32 (1991).

[23]F. Caupin and E. Herbert, "Cavitation in Water: A Review," *C. R. Phys*., **7**, 1000–17 (2006).

[24]S. H. Yang, M. Nosonovsky, H. Zhang, and K. H. Chung, "Nanoscale Water Capillary Bridges Under Deeply Negative Pressure," *Chem. Phys. Lett*., **451** [1–3] 88–92 (2008).

[25]F. Caupin, E. Herbert, S. Balibar, and M. W. Cole, "Comment on Nanoscale Water Capillary Bridges Under Deeply Negative Pressure," *Chem. Phys. Lett*., **463** [1–3] 283–5 (2008).

[26]K. Han, M. Ciccotti, and S. Roux, "Measuring Nanoscale Stress Intensity Factors with an Atomic Force Microscope," *Europhys. Lett*., **89** [6] 66003 (2010).

[27]G. Pallares, L. Ponson, A. Grimaldi, M. George, G. Prevot, and M. Ciccotti, "Crack Opening Profile in DCDC Specimen," *Int. J. Fract*., **156** [1] 11–20 (2009).

[28]M. L. Williams, "On the Stress Distribution at the Base of a Stationary Crack," *ASME J. Appl. Mech*., **24**, 109–14 (1957).

[29]H. F. Bueckner, "A Novel Principle for the Computation of Stress Intensity Factors," *Z. Angew. Math. Mech*., **50** [9] 52946 (1970).

[30]T. Fett, G. Rizzi, J. P. Guin, J. M. Lopez-Cepero, and S. M. Wiederhorn, "A Fracture Mechanics Analysis of the Double Cleavage Drilled Compression Test Specimen," *Eng. Frac. Mech*., **76** [7] 921–34 (2009). □